

Measurement of Jet Shapes in High- Q^2 Deep Inelastic Scattering at HERA

ZEUS Collaboration

Abstract

The shapes of jets with transverse energies, E_T^{jet} , up to 45 GeV produced in neutral- and charged-current deep inelastic e^+p scattering (DIS) at $Q^2 > 100 \text{ GeV}^2$ have been measured with the ZEUS detector at HERA. Jets are identified using a cone algorithm in the $\eta - \varphi$ plane with a cone radius of one unit. The jets become narrower as E_T^{jet} increases. The jet shapes in neutral- and charged-current DIS are found to be very similar. The jets in neutral-current DIS are narrower than those in resolved processes in photoproduction and closer to those in direct-photon processes for the same ranges in E_T^{jet} and jet pseudorapidity. The jet shapes in DIS are observed to be similar to those in e^+e^- interactions and narrower than those in $\bar{p}p$ collisions for comparable E_T^{jet} . Since the jets in e^+e^- interactions and e^+p DIS are predominantly quark initiated in both cases, the similarity in the jet shapes indicates that the pattern of QCD radiation within a quark jet is to a large extent independent of the hard scattering process in these reactions.

The ZEUS Collaboration

J. Breitweg, M. Derrick, D. Krakauer, S. Magill, D. Mikunas, B. Musgrave, J. Repond, R. Stanek,
R.L. Talaga, R. Yoshida, H. Zhang
Argonne National Laboratory, Argonne, IL, USA ^p

M.C.K. Mattingly
Andrews University, Berrien Springs, MI, USA

F. Anselmo, P. Antonioli, G. Bari, M. Basile, L. Bellagamba, D. Boscherini, A. Bruni, G. Bruni,
G. Cara Romeo, G. Castellini¹, L. Cifarelli², F. Cindolo, A. Contin, N. Coppola, M. Corradi,
S. De Pasquale, P. Giusti, G. Iacobucci, G. Laurenti, G. Levi, A. Margotti, T. Massam,
R. Nania, F. Palmonari, A. Pesci, A. Polini, G. Sartorelli, Y. Zamora Garcia³, A. Zichichi
University and INFN Bologna, Bologna, Italy ^f

C. Amelung, A. Bornheim, I. Brock, K. Coböken, J. Crittenden, R. Deffner, M. Eckert,
M. Grothe, H. Hartmann, K. Heinloth, L. Heinz, E. Hilger, H.-P. Jakob, A. Kappes, U.F. Katz,
R. Kerger, E. Paul, M. Pfeiffer, J. Stamm⁴, R. Wedemeyer⁵, H. Wieber
Physikalisches Institut der Universität Bonn, Bonn, Germany ^c

D.S. Bailey, S. Campbell-Robson, W.N. Cottingham, B. Foster, R. Hall-Wilton, G.P. Heath,
H.F. Heath, J.D. McFall, D. Piccioni, D.G. Roff, R.J. Tapper
H.H. Wills Physics Laboratory, University of Bristol, Bristol, U.K. ^o

R. Ayad, M. Capua, A. Garfagnini, L. Iannotti, M. Schioppa, G. Susinno
Calabria University, Physics Dept.and INFN, Cosenza, Italy ^f

J.Y. Kim, J.H. Lee, I.T. Lim, M.Y. Pac⁶
Chonnam National University, Kwangju, Korea ^h

A. Caldwell⁷, N. Cartiglia, Z. Jing, W. Liu, B. Mellado, J.A. Parsons, S. Ritz⁸, S. Sampson,
F. Sciulli, P.B. Straub, Q. Zhu
Columbia University, Nevis Labs., Irvington on Hudson, N.Y., USA ^q

P. Borzemeski, J. Chwastowski, A. Eskreys, J. Figiel, K. Klimek, M.B. Przybycień, L. Zawiejski
Inst. of Nuclear Physics, Cracow, Poland ^j

L. Adamczyk⁹, B. Bednarek, M. Bukowy, A.M. Czermak, K. Jeleń, D. Kisielewska,
T. Kowalski, M. Przybycień, E. Rulikowska-Zarębska, L. Suszycki, J. Zajac
Faculty of Physics and Nuclear Techniques, Academy of Mining and Metallurgy, Cracow, Poland ^j

Z. Duliński, A. Kotański
Jagellonian Univ., Dept. of Physics, Cracow, Poland ^k

G. Abbiendi¹⁰, L.A.T. Bauerdick, U. Behrens, H. Beier, J.K. Bienlein, G. Cases¹¹, K. Desler,
G. Drews, U. Fricke, I. Gialas¹², F. Goebel, P. Göttlicher, R. Graciani, T. Haas, W. Hain,
D. Hasell¹³, K. Hebbel, K.F. Johnson¹⁴, M. Kasemann, W. Koch, U. Kötz, H. Kowalski,
L. Lindemann, B. Löhr, J. Milewski, T. Monteiro¹⁵, J.S.T. Ng¹⁶, D. Notz, I.H. Park¹⁷,
A. Pellegrino, F. Pelucchi, K. Piotrkowski, M. Rohde, J. Roldán¹⁸, J.J. Ryan¹⁹, A.A. Savin,
U. Schneekloth, O. Schwarzer, F. Selonke, S. Stonjek, B. Surrow²⁰, E. Tassi, D. Westphal,
G. Wolf, U. Wollmer, C. Youngman, W. Zeuner
Deutsches Elektronen-Synchrotron DESY, Hamburg, Germany

B.D. Burow, C. Coldewey, H.J. Grabosch, A. Meyer, S. Schlenstedt
DESY-IfH Zeuthen, Zeuthen, Germany

G. Barbagli, E. Gallo, P. Pelfer
University and INFN, Florence, Italy^f

G. Maccarrone, L. Votano
INFN, Laboratori Nazionali di Frascati, Frascati, Italy^f

A. Bamberger, S. Eisenhardt, P. Markun, H. Raach, T. Trefzger²¹, S. Wölfle
Fakultät für Physik der Universität Freiburg i.Br., Freiburg i.Br., Germany^c

J.T. Bromley, N.H. Brook, P.J. Bussey, A.T. Doyle²², N. Macdonald, D.H. Saxon, L.E. Sinclair,
E. Strickland, R. Waugh
Dept. of Physics and Astronomy, University of Glasgow, Glasgow, U.K.^o

I. Bohnet, N. Gendner, U. Holm, A. Meyer-Larsen, H. Salehi, K. Wick
Hamburg University, I. Institute of Exp. Physics, Hamburg, Germany^c

L.K. Gladilin²³, D. Horstmann, D. Kçira²⁴, R. Klanner, E. Lohrmann, G. Poelz, W. Schott¹⁹,
F. Zetsche
Hamburg University, II. Institute of Exp. Physics, Hamburg, Germany^c

T.C. Bacon, I. Butterworth, J.E. Cole, G. Howell, L. Lamberti²⁵, K.R. Long, D.B. Miller,
N. Pavel, A. Priniias²⁶, J.K. Sedgbeer, D. Sideris, R. Walker
Imperial College London, High Energy Nuclear Physics Group, London, U.K.^o

U. Mallik, S.M. Wang, J.T. Wu
University of Iowa, Physics and Astronomy Dept., Iowa City, USA^p

P. Cloth, D. Filges
Forschungszentrum Jülich, Institut für Kernphysik, Jülich, Germany

J.I. Fleck²⁰, T. Ishii, M. Kuze, I. Suzuki²⁷, K. Tokushuku, S. Yamada, K. Yamauchi, Y. Yamazaki²⁸
Institute of Particle and Nuclear Studies, KEK, Tsukuba, Japan^g

S.J. Hong, S.B. Lee, S.W. Nam²⁹, S.K. Park
Korea University, Seoul, Korea^h

F. Barreiro, J.P. Fernández, G. García, C. Glasman³⁰, J.M. Hernández, L. Hervás²⁰, L. Labarga,
M. Martínez, J. del Peso, J. Puga, J. Terrón, J.F. de Trocóniz
Univer. Autónoma Madrid, Depto de Física Teórica, Madrid, Spainⁿ

F. Corriveau, D.S. Hanna, J. Hartmann, L.W. Hung, W.N. Murray, A. Ochs, M. Riveline,
D.G. Stairs, M. St-Laurent, R. Ullmann
McGill University, Dept. of Physics, Montréal, Québec, Canada^{a, b}

T. Tsurugai
Meiji Gakuin University, Faculty of General Education, Yokohama, Japan

V. Bashkirov, B.A. Dolgoshein, A. Stifutkin
Moscow Engineering Physics Institute, Moscow, Russia^l

G.L. Bashindzhagyan, P.F. Ermolov, Yu.A. Golubkov, L.A. Khein, N.A. Korotkova,
I.A. Korzhavina, V.A. Kuzmin, O.Yu. Lukina, A.S. Proskuryakov, L.M. Shcheglova³¹,
A.N. Solomin³¹, S.A. Zotkin

Moscow State University, Institute of Nuclear Physics, Moscow, Russia^m

C. Bokel, M. Botje, N. Brümmer, J. Engelen, E. Koffeman, P. Kooijman, A. van Sighem,
H. Tiecke, N. Tuning, W. Verkerke, J. Vosseveld, L. Wiggers, E. de Wolf

NIKHEF and University of Amsterdam, Amsterdam, Netherlandsⁱ

D. Acosta³², B. Bylsma, L.S. Durkin, J. Gilmore, C.M. Ginsburg, C.L. Kim, T.Y. Ling,
P. Nylander, T.A. Romanowski³³

Ohio State University, Physics Department, Columbus, Ohio, USA^p

H.E. Blaikley, R.J. Cashmore, A.M. Cooper-Sarkar, R.C.E. Devenish, J.K. Edmonds,
J. Große-Knetter³⁴, N. Harnew, C. Nath, V.A. Noyes³⁵, A. Quadt, O. Ruske, J.R. Tickner²⁶,
H. Uijterwaal, R. Walczak, D.S. Waters

Department of Physics, University of Oxford, Oxford, U.K.^o

A. Bertolin, R. Brugnera, R. Carlin, F. Dal Corso, U. Dosselli, S. Limentani, M. Morandin,
M. Posocco, L. Stanco, R. Stroili, C. Voci

Dipartimento di Fisica dell' Università and INFN, Padova, Italy^f

J. Bulmahn, B.Y. Oh, J.R. Okrasinski, W.S. Toothacker, J.J. Whitmore

Pennsylvania State University, Dept. of Physics, University Park, PA, USA^q

Y. Iga

Polytechnic University, Sagamihara, Japan^g

G. D'Agostini, G. Marini, A. Nigro, M. Raso

Dipartimento di Fisica, Univ. 'La Sapienza' and INFN, Rome, Italy^f

J.C. Hart, N.A. McCubbin, T.P. Shah

Rutherford Appleton Laboratory, Chilton, Didcot, Oxon, U.K.^o

D. Epperson, C. Heusch, J.T. Rahn, H.F.-W. Sadrozinski, A. Seiden, R. Wichmann, D.C. Williams
University of California, Santa Cruz, CA, USA^p

H. Abramowicz³⁶, G. Briskin, S. Dagan³⁷, S. Kananov³⁷, A. Levy³⁷

*Raymond and Beverly Sackler Faculty of Exact Sciences, School of Physics, Tel-Aviv University,
Tel-Aviv, Israel^e*

T. Abe, T. Fusayasu, M. Inuzuka, K. Nagano, K. Umemori, T. Yamashita

Department of Physics, University of Tokyo, Tokyo, Japan^g

R. Hamatsu, T. Hirose, K. Homma³⁸, S. Kitamura³⁹, T. Matsushita

Tokyo Metropolitan University, Dept. of Physics, Tokyo, Japan^g

M. Arneodo, R. Cirio, M. Costa, M.I. Ferrero, S. Maselli, V. Monaco, C. Peroni, M.C. Petrucci,
M. Ruspa, R. Sacchi, A. Solano, A. Staiano

Università di Torino, Dipartimento di Fisica Sperimentale and INFN, Torino, Italy^f

M. Dardo

II Faculty of Sciences, Torino University and INFN - Alessandria, Italy^f

D.C. Bailey, C.-P. Fagerstroem, R. Galea, G.F. Hartner, K.K. Joo, G.M. Levman, J.F. Martin, R.S. Orr, S. Polenz, A. Sabetfakhri, D. Simmons, R.J. Teuscher²⁰
University of Toronto, Dept. of Physics, Toronto, Ont., Canada^a

J.M. Butterworth, C.D. Catterall, M.E. Hayes, T.W. Jones, J.B. Lane, R.L. Saunders, M.R. Sutton, M. Wing
University College London, Physics and Astronomy Dept., London, U.K.^o

J. Ciborowski, G. Grzelak⁴⁰, M. Kasprzak, R.J. Nowak, J.M. Pawlak, R. Pawlak, T. Tymieniecka, A.K. Wróblewski, J.A. Zakrzewski, A.F. Żarnecki
Warsaw University, Institute of Experimental Physics, Warsaw, Poland^j

M. Adamus
Institute for Nuclear Studies, Warsaw, Poland^j

O. Deppe, Y. Eisenberg³⁷, D. Hochman, U. Karshon³⁷
Weizmann Institute, Department of Particle Physics, Rehovot, Israel^d

W.F. Badgett, D. Chapin, R. Cross, S. Dasu, C. Foudas, R.J. Loveless, S. Mattingly, D.D. Reeder, W.H. Smith, A. Vaiciulis, M. Wodarczyk
University of Wisconsin, Dept. of Physics, Madison, WI, USA^p

A. Deshpande, S. Dhawan, V.W. Hughes
Yale University, Department of Physics, New Haven, CT, USA^p

S. Bhadra, W.R. Frisken, M. Khakzad, W.B. Schmidke
York University, Dept. of Physics, North York, Ont., Canada^a

¹ also at IROE Florence, Italy
² now at Univ. of Salerno and INFN Napoli, Italy
³ supported by Worldlab, Lausanne, Switzerland
⁴ now at C. Plath GmbH, Hamburg
⁵ retired
⁶ now at Dongshin University, Naju, Korea
⁷ also at DESY
⁸ Alfred P. Sloan Foundation Fellow
⁹ supported by the Polish State Committee for Scientific Research, grant No. 2P03B14912
¹⁰ now at INFN Bologna
¹¹ now at SAP A.G., Walldorf
¹² now at Univ. of Crete, Greece
¹³ now at Massachusetts Institute of Technology, Cambridge, MA, USA
¹⁴ visitor from Florida State University
¹⁵ supported by European Community Program PRAXIS XXI
¹⁶ now at DESY-Group FDET
¹⁷ visitor from Kyungpook National University, Taegu, Korea, partially supported by DESY
¹⁸ now at IFIC, Valencia, Spain
¹⁹ now a self-employed consultant
²⁰ now at CERN
²¹ now at ATLAS Collaboration, Univ. of Munich
²² also at DESY and Alexander von Humboldt Fellow at University of Hamburg
²³ on leave from MSU, supported by the GIF, contract I-0444-176.07/95
²⁴ supported by DAAD, Bonn
²⁵ supported by an EC fellowship
²⁶ PPARC Post-doctoral Fellow
²⁷ now at Osaka Univ., Osaka, Japan
²⁸ supported by JSPS Postdoctoral Fellowships for Research Abroad
²⁹ now at Wayne State University, Detroit
³⁰ supported by an EC fellowship number ERBFMBICT 972523
³¹ partially supported by the Foundation for German-Russian Collaboration DFG-RFBR
(grant no. 436 RUS 113/248/3 and no. 436 RUS 113/248/2)
³² now at University of Florida, Gainesville, FL, USA
³³ now at Department of Energy, Washington
³⁴ supported by the Feodor Lynen Program of the Alexander von Humboldt foundation
³⁵ Glasstone Fellow
³⁶ an Alexander von Humboldt Fellow at University of Hamburg
³⁷ supported by a MINERVA Fellowship
³⁸ now at ICEPP, Univ. of Tokyo, Tokyo, Japan
³⁹ present address: Tokyo Metropolitan College of Allied Medical Sciences, Tokyo 116, Japan
⁴⁰ supported by the Polish State Committee for Scientific Research, grant No. 2P03B09308

- a* supported by the Natural Sciences and Engineering Research Council of Canada (NSERC)
- b* supported by the FCAR of Québec, Canada
- c* supported by the German Federal Ministry for Education and Science, Research and Technology (BMBF), under contract numbers 057BN19P, 057FR19P, 057HH19P, 057HH29P
- d* supported by the MINERVA Gesellschaft für Forschung GmbH, the German Israeli Foundation, the U.S.-Israel Binational Science Foundation, and by the Israel Ministry of Science
- e* supported by the German-Israeli Foundation, the Israel Science Foundation, the U.S.-Israel Binational Science Foundation, and by the Israel Ministry of Science
- f* supported by the Italian National Institute for Nuclear Physics (INFN)
- g* supported by the Japanese Ministry of Education, Science and Culture (the Monbusho) and its grants for Scientific Research
- h* supported by the Korean Ministry of Education and Korea Science and Engineering Foundation
- i* supported by the Netherlands Foundation for Research on Matter (FOM)
- j* supported by the Polish State Committee for Scientific Research, grant No. 115/E-343/SPUB/P03/002/97, 2P03B10512, 2P03B10612, 2P03B14212, 2P03B10412
- k* supported by the Polish State Committee for Scientific Research (grant No. 2P03B08308) and Foundation for Polish-German Collaboration
- l* partially supported by the German Federal Ministry for Education and Science, Research and Technology (BMBF)
- m* supported by the Fund for Fundamental Research of Russian Ministry for Science and Education and by the German Federal Ministry for Education and Science, Research and Technology (BMBF)
- n* supported by the Spanish Ministry of Education and Science through funds provided by CICYT
- o* supported by the Particle Physics and Astronomy Research Council
- p* supported by the US Department of Energy
- q* supported by the US National Science Foundation

1 Introduction

The internal structure of a jet is expected to depend mainly on the type of primary parton, quark or gluon, from which it originated and to a lesser extent on the particular hard scattering process. For cone jet algorithms [1, 2] a useful representation of the jet's internal structure is given by the jet shape [3]. At sufficiently high jet energy, where fragmentation effects become negligible, the jet shape should be calculable by perturbative Quantum Chromodynamics (pQCD). pQCD predicts gluon jets to be broader than quark jets as a consequence of the gluon-gluon coupling strength being larger than that of the quark-gluon coupling [4]. Measurements of the jet width in e^+e^- interactions at LEP1 have shown that gluon jets are indeed broader than quark jets [5]. The dependence of the structure of quark and gluon jets on the production process can be investigated by comparing measurements of the jet shape in different reactions in which the final-state jets are predominantly quark or gluon initiated.

Measurements of the integrated jet shape were made in $\bar{p}p$ collisions at $\sqrt{s} = 1.8$ TeV using charged particles [6] as well as both neutral and charged particles [7], and a qualitative agreement with $O(\alpha_s^3)$ QCD calculations [3, 8] was found. Measurements of the integrated and differential jet shapes were made in e^+e^- interactions at LEP1 using both neutral and charged particles [9] and were found to be well described by leading-logarithm parton-shower Monte Carlo calculations. It was observed [9] that the jets in e^+e^- are significantly narrower than those in $\bar{p}p$ and most of this difference was ascribed to the different mixtures of quark and gluon jets in the two production processes.

Measurements of the integrated jet shape in quasi-real photon proton collisions at HERA have recently been presented [10] and were found to be well described by leading-logarithm parton-shower Monte Carlo calculations except for the inclusive production of jets with high jet pseudorapidity (η^{jet}) and low jet transverse energy (E_T^{jet}). Fixed-order perturbative QCD calculations at the parton level [11] are able to describe the measured jet shapes within the uncertainties on the matching between the theoretical and experimental jet algorithms.

At HERA, jet production has been observed in both neutral- [12, 13] and charged-current [14] deep inelastic ep scattering (DIS) at large Q^2 (where Q^2 is the virtuality of the exchanged boson). In this paper, measurements of the differential and integrated jet shapes in neutral- and charged-current DIS at $Q^2 > 100$ GeV² are presented. The data sample used in this analysis has been collected with the ZEUS detector in e^+p interactions at the HERA collider. To compare with measurements of the jet shapes in $\bar{p}p$, γp and e^+e^- collisions, jets are searched for with an iterative cone algorithm [10] with radius $R = 1$ in the pseudorapidity¹ (η) - azimuth (φ) plane of the laboratory frame. Jets have been selected with jet transverse (with respect to the proton beam direction) energy $E_T^{jet} > 14$ GeV and jet pseudorapidity in the range $-1 < \eta^{jet} < 2$. The jet shape has been measured using the ZEUS calorimeter and corrected to the hadron level. The measurements are presented as functions of E_T^{jet} and η^{jet} . The measured jet shapes are compared to similar measurements in other reactions and to leading-logarithm parton-shower Monte Carlo calculations.

¹The ZEUS coordinate system is defined as right-handed with the Z -axis pointing in the proton beam direction, hereafter referred to as forward, and the X -axis horizontal, pointing towards the centre of HERA. The pseudorapidity is defined as $\eta = -\ln(\tan \frac{\theta}{2})$, where the polar angle θ is taken with respect to the proton beam direction.

2 Experimental setup

During 1995 and 1996 HERA operated with protons of energy $E_p = 820$ GeV and positrons of energy $E_e = 27.5$ GeV. The ZEUS detector is described in detail in [15, 16]. The main subdetectors used in the present analysis are the central tracking system positioned in a 1.43 T solenoidal magnetic field and the uranium-scintillator sampling calorimeter (CAL). The tracking system was used to establish an interaction vertex and to select neutral- and charged-current DIS events. The CAL is hermetic and consists of 5918 cells each read out by two photomultiplier tubes. Under test beam conditions the CAL has energy resolutions of $18\%/\sqrt{E}$ for electrons and $35\%/\sqrt{E}$ for hadrons. Energy deposits in the CAL were used to identify the scattered positron, to find jets and to measure jet energies. Jet energies are corrected for the energy lost in inactive material in front of the CAL. This material is typically about one radiation length. The effects of uranium noise were minimised by discarding cells in the electromagnetic (EMC) or hadronic (HAC) sections if they had energy deposits of less than 60 MeV or 110 MeV, respectively. A three-level trigger was used to select events online [14, 16, 17].

3 Data selection

Neutral-current (NC) DIS events have been selected offline from the ZEUS 1995 data sample, which corresponds to an integrated luminosity of 6.3 pb^{-1} , using criteria similar to those reported previously [17, 18]. The main steps are briefly discussed here. The scattered positron candidate has been identified by using the pattern of energy deposits in the CAL [19]. The energy ($E_{e'}$) and polar angle ($\theta_{e'}$) of the positron candidate have been determined from the CAL measurements. The Q^2 variable has been reconstructed by the double-angle method (Q_{DA}^2) [20], which uses $\theta_{e'}$ and an angle that corresponds to the direction of the scattered quark in quark-parton model type events. This second angle has been determined from the CAL measurements of the hadronic final state. The following requirements have been imposed:

- A positron candidate of uncorrected energy $E_{e'} > 10$ GeV. This cut ensures a high and well understood positron finding efficiency and suppresses background from photoproduction events, where the scattered positron escapes down the rear beampipe.
- $y_e < 0.95$, where $y_e = 1 - E_{e'}(1 - \cos \theta_{e'})/(2E_e)$. This condition removes events where fake positron candidates are found in the forward region of the CAL.
- The total energy not associated with the positron candidate within a cone of radius 0.7 units in the $\eta - \varphi$ plane around the positron direction must be less than 5 GeV. This condition removes photoproduction and DIS events where part of a jet has been falsely identified as the scattered positron.
- A track is required to match the positron candidate identified in the CAL for $\eta_e < 2$, where η_e is the pseudorapidity of the positron candidate. This requirement suppresses cosmic rays, beam-halo muons, photoproduction and DIS events where an electromagnetic shower in the CAL has been falsely identified as the scattered positron.
- For $\eta_e > 2$ the transverse energy of the positron candidate should be larger than 20 GeV. This requirement further reduces the number of fake positrons in the forward region of the CAL.

- $38 \text{ GeV} < (E - p_Z) < 65 \text{ GeV}$, where E is the total energy as measured by the CAL, $E = \sum_i E_i$, and p_Z is the Z -component of the vector $\vec{p} = \sum_i E_i \vec{r}_i$; in both cases the sum runs over all CAL cells, E_i is the energy of the calorimeter cell i and \vec{r}_i is a unit vector along the line joining the reconstructed vertex and the geometric centre of the cell i . This cut removes events with large initial-state radiation and further reduces the background from photoproduction.
- Events have been removed from the sample if there was a second positron candidate with energy above 10 GeV and without a track match, and the energy in the CAL after subtracting that of the two positron candidates is below 10 GeV. This requirement removes elastic Compton scattering events ($ep \rightarrow e\gamma p$).
- $\cancel{P}_t / \sqrt{E_t} < 3 \text{ GeV}^{1/2}$ where \cancel{P}_t is the missing transverse momentum as measured with the CAL ($\cancel{P}_t \equiv \sqrt{p_X^2 + p_Y^2}$) and E_t is the total transverse energy in the CAL. This cut removes cosmic rays and beam-related background.
- The vertex position along the beam axis must be in the range $-30 < Z < 36 \text{ cm}$.
- $Q_{DA}^2 > 100 \text{ GeV}^2$.

Charged-current (CC) DIS events have been selected offline from the ZEUS 1995 and 1996 data samples, which correspond to an integrated luminosity of 14.8 pb^{-1} , using criteria similar to those reported in [14]. The Q^2 variable has been determined using the method of Jacquet-Blondel (Q_{JB}^2) [21], which uses the information from the hadronic energy flow of the event. The following conditions have been imposed:

- $\cancel{P}_t > 11 \text{ GeV}$. This cut ensures high trigger efficiency.
- $\cancel{P}_t / E_t > 0.5$. This cut rejects photoproduction and beam-related background.
- The vertex position along the beam axis should lie in the range $-30 < Z < 36 \text{ cm}$.
- At least one track should point to the vertex. This requirement rejects cosmic rays and beam-gas interactions.
- The number of tracks not associated to the vertex must be less than 20% of the total number of tracks. This cut further reduces the background from beam-gas interactions.
- The difference $\Delta\varphi$ between the azimuths of the net transverse momentum as measured by the tracks associated with the vertex and as measured by the CAL has been required to fulfill $|\Delta\varphi| < 1 \text{ rad}$. This requirement removes overlays of cosmic rays on ep interactions.
- $P_t^{tracks} / \cancel{P}_t > 0.1$, where P_t^{tracks} is the net transverse momentum of the tracks associated with the vertex (this condition has not been applied if $\cancel{P}_t > 25 \text{ GeV}$). This cut rejects beam-related background, in which \cancel{P}_t is pointing to small polar angles, and events with additional non- ep related energy deposits in the CAL (mainly cosmic rays).
- The event has been removed from the sample if there was an isolated positron candidate with energy above 10 GeV and a track match. This condition removes NC DIS events.
- Pattern recognition algorithms based on the topology of the CAL energy distribution were applied to reject cosmic rays and beam-halo muons.

- $Q_{corr}^2 > 100 \text{ GeV}^2$, where Q_{corr}^2 denotes the corrected value of Q_{JB}^2 as described in [14]. The resolution in the reconstruction of Q^2 is $\approx 25\%$.

A search for jet structure using the CAL cells (see Section 5) has been performed on both samples (NC and CC DIS), and events with at least one jet of ‘corrected’ transverse energy (see Section 5) $E_T^{jet} > 14 \text{ GeV}$ and $-1 < \eta^{jet} < 2$ have been retained. The selected sample of NC (CC) DIS consists of 6926 (231) events containing 7092 (233) jets. In both cases, the background from photoproduction has been estimated using Monte Carlo techniques and was found to be below 1%.

4 Monte Carlo simulation

The response of the detector to jets and the correction factors for the jet shapes have been determined from samples of Monte Carlo (MC) events.

NC and CC DIS events have been generated using the LEPTO program [22] interfaced to HERACLES [23] via DJANGO [24]. The HERACLES program includes photon and Z^o exchanges and first-order electroweak radiative corrections. The CTEQ4D [25] NLO proton parton densities have been used. The hadronic final state is simulated using the colour-dipole model [26] including the leading-order (LO) QCD diagrams as implemented in ARIADNE [27] for the QCD cascade. As an alternative, samples of events have been generated using the model of LEPTO based on first-order QCD matrix elements plus parton-shower (MEPS). For the generation of the samples with MEPS, the soft colour interactions option has been switched off.

In addition, a sample of NC DIS events has been generated using the PYTHIA program [28]: a lowest-order electroweak calculation including initial- and final-state QCD radiation in the leading-logarithm parton-shower approximation. In this case, events have been generated using the MRSA [29] set of proton parton densities and the first-order QCD matrix elements have not been included. In all cases, the LUND string model [30] as implemented in JETSET [28] is used for modelling the fragmentation into hadrons.

All MC generated events have been passed through the ZEUS detector and trigger simulation programs [16]. They have been reconstructed and analysed by the same program chain as the data.

5 Jet search and energy corrections

An iterative cone algorithm in the $\eta - \varphi$ plane [1, 2] is used to reconstruct jets from the energy measured in the CAL cells for both data and MC generated events, and also from the final-state hadrons for MC generated events. A detailed description of the algorithm can be found in [10]. The jets reconstructed from the CAL cell energies are called *cal* jets and the variables associated with them are denoted by $E_{T,cal}^{jet}$, η_{cal}^{jet} and φ_{cal}^{jet} . The axis of the jet is defined according to the Snowmass convention [2], where η_{cal}^{jet} (φ_{cal}^{jet}) is the transverse-energy weighted mean pseudorapidity (azimuth) of all the CAL cells belonging to that jet. The energy sharing of overlapping jets is dealt with using the following procedure. Two jets are merged if the overlapping energy exceeds 75% of the total energy of the jet with the lower energy; otherwise two different jets are formed and the common cells are assigned to the nearest jet. The cone radius R used in the jet search is set equal to 1.

For the MC generated events, the same jet algorithm is also applied to the final-state particles. The jets found are called *hadron* jets and the variables associated with them are denoted

by $E_{T,had}^{jet}$, η_{had}^{jet} , and φ_{had}^{jet} . *Hadron* jets with $E_{T,had}^{jet} > 14$ GeV and $-1 < \eta_{had}^{jet} < 2$ are selected.

The comparison of the reconstructed jet variables between the *hadron* and the *cal* jets in MC generated events [31] shows no significant systematic shift in the angular variables η_{cal}^{jet} and φ_{cal}^{jet} with respect to η_{had}^{jet} and φ_{had}^{jet} . However, the transverse energy of the *cal* jet underestimates that of the *hadron* jet by an average amount of $\approx 16\%$ with an r.m.s. of 11%. This effect is due mainly to energy losses in the inactive material in front of the CAL and is corrected for using the following procedure. The transverse energy corrections to *cal* jets averaged over the azimuthal angle are determined using the samples of MC generated events [31]. These corrections are constructed as multiplicative factors, $C(E_{T,cal}^{jet}, \eta_{cal}^{jet})$, which, when applied to the E_T of the *cal* jets, give the ‘corrected’ transverse energies of the jets, $E_T^{jet} = C(E_{T,cal}^{jet}, \eta_{cal}^{jet}) \times E_{T,cal}^{jet}$ [31].

6 Jet shape

The differential jet shape is defined as the average fraction of the jet’s transverse energy that lies inside an annulus in the $\eta - \varphi$ plane of inner (outer) radius $r - \Delta r/2$ ($r + \Delta r/2$) concentric with the jet defining cone [3]:

$$\rho(r) = \frac{1}{N_{jets}} \frac{1}{\Delta r} \sum_{jets} \frac{E_T(r - \Delta r/2, r + \Delta r/2)}{E_T(0, R)}, \quad (1)$$

where $E_T(r - \Delta r/2, r + \Delta r/2)$ is the transverse energy within the given annulus and N_{jets} is the total number of jets in the sample. The differential jet shape has been measured for r values varying from 0.05 to 0.95 in $\Delta r = 0.1$ increments. The integrated jet shape defined by

$$\psi(r) = \frac{1}{N_{jets}} \sum_{jets} \frac{E_T(0, r)}{E_T(0, R)} \quad (2)$$

is also used. By definition, $\psi(R) = 1$. It has been measured for r values varying from 0.1 to 1.0 in $\Delta r = 0.1$ increments.

The following procedure is used to reconstruct the differential jet shape from the CAL cells in data and MC generated events: for each jet the sum of the transverse energies of the CAL cells assigned to the jet, $E_{T,cal}(r - \Delta r/2, r + \Delta r/2)$, with a distance $r' = \sqrt{(\Delta\eta)^2 + (\Delta\varphi)^2}$ to the jet axis between $r - \Delta r/2$ and $r + \Delta r/2$ is determined and divided by $E_{T,cal}(0, 1)$. The differential jet shape as measured with the CAL, $\rho_{cal}(r)$, is then defined in analogy with eq. (1), where the sum now runs over all the *cal* jets in the selected sample and N_{jets} is the total number of *cal* jets in the sample. Similarly, the integrated jet shape as measured with the CAL, $\psi_{cal}(r)$, is defined in analogy with eq. (2).

The same jet shape definition as used above for the CAL cells is applied to the final-state particles in the case of MC generated events and the resulting differential (integrated) jet shape is denoted by $\rho_{had}^{MC}(r)$ ($\psi_{had}^{MC}(r)$).

6.1 Jet shape correction

The differential and integrated jet shapes as measured with the CAL are corrected back to the hadron level using the samples of MC generated events. The corrected differential and integrated jet shapes, $\rho(r)$ and $\psi(r)$, refer to jets at the hadron level with a cone radius of one unit in the $\eta - \varphi$ plane. The measurements are given for jets with $E_T^{jet} > 14$ GeV and $-1 < \eta^{jet} < 2$ in the kinematic region $Q^2 > 100$ GeV².

The corrected jet transverse energy is used only to select the sample of jets ($E_T^{jet} > 14$ GeV) and to study the dependence of the jet shape as a function of E_T^{jet} . The reconstructed jet shapes are then corrected for acceptance and smearing effects using the samples of MC generated events. The correction factors also take into account the efficiency of the trigger, the selection criteria, the purity and efficiency of the jet reconstruction, and the effects of the energy losses due to inactive material in front of the CAL. The corrected differential (integrated) jet shape is determined bin-by-bin as $\rho(r) = G_{cal}^{MC}(r) \cdot \rho_{cal}(r)$ and $\psi(r) = F_{cal}^{MC}(r) \cdot \psi_{cal}(r)$, where the correction factors are defined as $G_{cal}^{MC}(r) = \rho_{had}^{MC}(r)/\rho_{cal}^{MC}(r)$ and $F_{cal}^{MC}(r) = \psi_{had}^{MC}(r)/\psi_{cal}^{MC}(r)$ and are determined separately for each region of η^{jet} and E_T^{jet} .

For this approach to be valid, the uncorrected jet shapes in the data must be described by the MC simulations at the detector level. As shown later, this condition is satisfied by the ARIADNE and MEPS simulations in all η^{jet} and E_T^{jet} regions studied. The samples of events generated with ARIADNE are used to correct the jet shapes. The correction factors $G_{cal}^{MC}(r)$ do not show a strong dependence on η^{jet} or E_T^{jet} and vary between 0.7 and 1 for $r \geq 0.15$. The correction factors for the integrated jet shape $F_{cal}^{MC}(r)$ differ from unity by less than 25% for $r \geq 0.2$. Close to the centre of the jet the correction factor $G_{cal}^{MC}(r = 0.05) \equiv F_{cal}^{MC}(r = 0.1)$ is large and varies between 1.4 and 1.7 depending on η^{jet} and E_T^{jet} .

The jet shapes have been also reconstructed using tracks instead of CAL cells both in data and MC generated events. Since the use of tracks gives an improved spatial resolution for the transverse-energy flow of the charged particles within a jet, this study provides a cross-check of the resolution in r for the jet shape reconstructed using the CAL. The resulting corrected jet shapes are consistent with those using the CAL cells within the uncertainties of the measurements (see next section).

6.2 Systematic uncertainties

A detailed study of the sources contributing to the systematic uncertainties of the measurements has been carried out [32]. The uncertainties have been classified into four groups:

- The energy corrections to the jets and the correction functions to the jet shapes in NC and CC DIS have been evaluated using the MEPS generator. The changes induced in $\rho(r)$ are typically below 10%.
- The absolute energy scale of the *cal* jets in the MC generated events has been varied by $\pm 3\%$. The resulting corrected $\rho(r)$ changes typically by less than 3%.
- Variations in the simulation of the CAL response to low-energy particles yielded changes in $\rho(r)$ typically below 3%.
- Variations in the simulation of the trigger and a variation of the cuts used to select the data within the ranges allowed by the comparison between data and MC simulations resulted in negligible changes in the corrected jet shapes.

For the measurements of jet shapes in NC DIS, the statistical errors are negligible compared to the systematic uncertainties. Conversely, the statistical errors dominate in the CC DIS analysis. The total positive (negative) systematic uncertainty on $\rho(r)$ at each value of r has been determined by adding in quadrature the positive (negative) deviations from the central value. The systematic uncertainties have been added in quadrature to the statistical errors and are shown as error bars in the figures.

7 Results

7.1 Jet shapes in DIS

The differential and integrated jet shapes are measured for jets in the reactions

$$e^+p \rightarrow e^+(\bar{\nu}) + \text{jet} + X$$

with $Q^2 > 100 \text{ GeV}^2$. Jets are required to have $E_T^{jet} > 14 \text{ GeV}$ and $-1 < \eta^{jet} < 2$. There are 6018, 855 and 53 events in the NC DIS data sample with Q^2 in the range $100 - 1000 \text{ GeV}^2$, $1000 - 5000 \text{ GeV}^2$ and $5000 - 25000 \text{ GeV}^2$. The corresponding numbers for the CC DIS data sample are 84, 123 and 24 events.

Jet shapes in NC DIS

The measured differential jet shapes in NC DIS for different regions in η^{jet} and E_T^{jet} are shown in Figures 1 and 2, respectively. The differential jet shape exhibits a prominent peak at the centre of the jet. It decreases by a factor ≈ 40 from the centre of the jet ($r = 0.05$) to the edge of the jet ($r = 0.95$). Figure 3 shows the measured average fraction of the jet's transverse energy that lies inside an inner cone of radius $r = 0.5$ concentric with the jet defining cone, $\psi(r = 0.5)$, as functions of η^{jet} and E_T^{jet} . Note that $\psi(r = 0.5)$ has been measured in ranges of E_T^{jet} and the data points in Figure 3 (lower plot) are located at the weighted mean in each E_T^{jet} range. It is observed that the jets become narrower as E_T^{jet} increases. The measured $\psi(r = 0.5)$ exhibits no significant dependence on η^{jet} .

The predictions of ARIADNE, MEPS and PYTHIA are compared to the measured jet shapes in Figures 1 to 3. The predicted jet shape of the colour-dipole model (ARIADNE) describes the measured jet shape well in all η^{jet} and E_T^{jet} regions considered. The predicted jets of PYTHIA tend to be narrower at low E_T^{jet} than those in the data (see Figure 3). In the case of MEPS, the predicted jets show a tendency to be broader at low η^{jet} than those in the data.

Jet shapes in CC DIS

The results for $\rho(r)$ in CC DIS for different regions of E_T^{jet} are shown in Figure 4. The differential jet shape shows similar general features to those of the jets in NC DIS. Figure 5 shows the measured $\psi(r = 0.5)$ as functions of η^{jet} and E_T^{jet} . The measured $\psi(r = 0.5)$ exhibits no significant dependence on η^{jet} and its dependence on E_T^{jet} is similar to that observed in NC DIS. The predictions of ARIADNE and MEPS (see Figures 4 and 5) provide a reasonable description of the measured jet shape.

The measured jet shapes in NC DIS are compared with those in CC DIS in Figure 6 and found to be very similar in each region of E_T^{jet} . Measurements of the ratio of the differential jet shapes in CC and NC DIS, $\rho^{CC}(r)/\rho^{NC}(r)$, for the same regions of E_T^{jet} as above are also shown in Figure 6 (lower part of each plot) and found to be compatible with unity. In these measurements some of the systematic uncertainties common to NC and CC DIS cancel. The median of the Q^2 distribution has been determined for the NC and CC DIS samples of jets in each E_T^{jet} region: 310 GeV^2 (450 GeV^2) for $14 < E_T^{jet} < 21 \text{ GeV}$, 710 GeV^2 (1000 GeV^2) for $21 < E_T^{jet} < 29 \text{ GeV}$, 1260 GeV^2 (1600 GeV^2) for $29 < E_T^{jet} < 37 \text{ GeV}$ and 2000 GeV^2 (2200 GeV^2) for $37 < E_T^{jet} < 45 \text{ GeV}$ in the NC (CC) DIS samples of jets. Some differences are observed in the Q^2 distributions of the two processes for a given range in E_T^{jet} . As a cross-check, the jet shapes in NC and CC DIS have been measured in a common region of Q^2 for each range in E_T^{jet} and no significant difference has been found. Therefore, the observation that the jet

shapes in NC and CC DIS are very similar, for the same range of E_T^{jet} , is independent of the different Q^2 distributions in these processes.

7.2 Comparison to jet shapes in photoproduction

In photoproduction, two types of QCD processes contribute to jet production at LO [33, 34]: either the photon interacts directly with a parton in the proton (direct process) or the photon acts as a source of partons which interact with those in the proton (resolved process). It has been noted that resolved processes dominate jet photoproduction in the entire E_T^{jet} region studied [31]. In the case of dijet photoproduction the contributions of resolved and direct processes can be separated [35] by using the variable $x_\gamma^{OBS} = (\sum_{jets} E_T^{jet} e^{-\eta^{jet}})/(2E_\gamma)$, where the sum runs over the two jets of highest E_T^{jet} and E_γ is the initial photon energy. This variable represents the fraction of the photon's momentum participating in the production of the two jets with highest E_T^{jet} . The LO direct and resolved processes largely populate different regions of x_γ^{OBS} , with the direct processes being concentrated at high values.

In Figure 7 the measured integrated jet shape in NC DIS are compared to those in dijet photoproduction [10] for two different regions: $x_\gamma^{OBS} \geq 0.75$ and $x_\gamma^{OBS} < 0.75$. The comparison between the jet shapes in NC DIS and dijet photoproduction is made for the same ranges of η^{jet} and the E_T^{jet} spectrum is similar in these two processes. The jets produced in NC DIS are narrower than those in dijet photoproduction but closer to those dominated by direct processes ($x_\gamma^{OBS} \geq 0.75$). This comparison can be understood in terms of the large fraction of final-state quark jets expected in NC DIS ($e^+q \rightarrow e^+q$) and direct processes in photoproduction (dominated by the subprocess $\gamma g \rightarrow q\bar{q}$). The remaining differences may be attributed to the contribution from the direct subprocess $\gamma q \rightarrow qg$ and that of resolved processes, in which the jets are broader as shown by the measurements in dijet photoproduction with $x_\gamma^{OBS} < 0.75$.

7.3 Comparison to measurements in e^+e^- and $\bar{p}p$ collisions

The measured jet shape in NC (CC) DIS with $Q^2 > 100 \text{ GeV}^2$ for jets with transverse energy between 37 and 45 GeV, with a mean of 40 GeV (41 GeV), is compared to the measurements of the jet shape corrected to the hadron level in $\bar{p}p$ collisions by CDF [6] and DØ [7] and in e^+e^- interactions by OPAL [9]:

- The CDF data [6] have been obtained using an iterative cone algorithm with $R = 1$ similar to that used here. The measurements shown are for jets with transverse energy between 40 and 60 GeV, with a mean of 45 GeV, and pseudorapidity $0.1 < |\eta^{jet}| < 0.7$. The contribution to the jet shape due to the underlying event was found to be small². If a jet shares more than 75% of its energy with a jet of higher energy, the two are merged together; otherwise, they are defined as distinct and the particles common to both jets are assigned to the nearest jet.
- The DØ data [7] have been obtained also using an iterative cone algorithm with $R = 1$ similar to that used here. The jet direction was defined according to a convention different from that of Snowmass; however, this difference is not expected to have a significant effect on the results [36]. The jet shape has been measured for jets with transverse energy between 45 and 70 GeV, with a mean of 53 GeV, and pseudorapidity $|\eta^{jet}| < 0.2$. The jet shape has been corrected to remove the small contribution due to the underlying event.

²In NC and CC DIS the underlying event is not expected to contribute in the kinematic region studied here.

Two jets were merged if more than 50% of the E_T of the jet with smaller E_T was contained in the overlap region; otherwise, the two jets were not merged and each particle in the overlap region was assigned to the nearest jet.

- The OPAL data [9] have been obtained using a cone algorithm especially designed to emulate that of the CDF measurements, i.e. defining the cone in the $\eta - \varphi$ plane, using $R = 1$, demanding $|\eta^{jet}| < 0.7$ and measuring the transverse energy flow. The jet shape has been measured for jets with energy greater than 35 GeV, with a mean of 40.4 GeV. The e^+e^- data have no underlying event. Overlapping jets are treated using the same procedure as CDF.

The measured differential jet shapes in NC and CC DIS are compared to that measured in e^+e^- interactions in Figure 8 and are found to be similar. The ratio of the differential jet shapes in NC DIS and e^+e^- interactions, $\rho^{NC}(r)/\rho^{e^+e^-}(r)$, is also shown in Figure 8 (lower part of the figure) and is found to be compatible with unity within the uncertainties of the DIS measurements, which are dominant. For the selected samples of jets, the jet shapes in e^+e^- interactions and DIS are expected to be similar due to the large fraction of final-state quark jets in these two processes. However, some differences may appear since there are configurations of colour flow (for example, that of initial-state QCD radiation) in DIS which are not present in e^+e^- . The striking similarity in the jet shapes indicates the large extent to which the pattern of QCD radiation within a quark jet is independent of the hard scattering process in these reactions.

The measured integrated jet shapes in DIS are compared to those in e^+e^- interactions and $\bar{p}p$ collisions in Figure 9. The measured jets in DIS at HERA are found to be narrower than those in $\bar{p}p$ collisions. The measurements in $\bar{p}p$ collisions have been performed for jets with slightly higher energy than those in NC and CC DIS. This difference cannot explain the discrepancy in the jet shapes since the jets become narrower as the jet energy increases. As stated in [9], most of the difference between the jet shapes in e^+e^- interactions and $\bar{p}p$ collisions can be ascribed to the larger fraction of gluon jets in the latter reaction. The comparison between the measured jet shapes in DIS and $\bar{p}p$ collisions suggests that, also in this case, the difference can be attributed to differences between quark and gluon jet properties.

8 Summary and conclusions

Measurements have been presented of the differential and integrated jet shapes in neutral- and charged-current deep inelastic e^+p scattering at $\sqrt{s} = 300$ GeV using data collected by ZEUS in 1995 and 1996. The jet shapes refer to jets at the hadron level with a cone radius of one unit in the $\eta - \varphi$ plane and are given for the kinematic region $Q^2 > 100$ GeV². Jets with $E_T^{jet} > 14$ GeV and $-1 < \eta^{jet} < 2$ have been considered. The jets become narrower as E_T^{jet} increases. No significant η^{jet} dependence of the jet shape has been observed. The measured jet shapes in neutral- and charged-current DIS are found to be very similar.

The measurements of jet shapes have been compared to the predictions of Monte Carlo generators using different models for the QCD radiation. The colour-dipole model as implemented in ARIADNE provides a reasonable description of the measured jet shapes in all η^{jet} and E_T^{jet} regions studied. The parton-shower approach without first-order QCD matrix-elements predict jets which are slightly narrower at low E_T^{jet} than those in the data for all the η^{jet} regions studied. The inclusion of first-order QCD matrix-elements improves the description of the data for $\eta^{jet} > 1$, but leads to jets which are slightly broader for $\eta^{jet} < 1$.

The jets in neutral-current DIS are narrower than those in dijet photoproduction but closer to those in direct-photon processes for the same ranges in jet transverse energy and pseudorapidity. The jets in DIS are found to be narrower than those in $\bar{p}p$ collisions. This difference can be attributed to a larger contribution of gluon jets in $\bar{p}p$ collisions. The measured jet shapes in neutral- and charged-current DIS are similar to those in e^+e^- interactions for comparable ranges of jet transverse energy. Since the jets in e^+e^- interactions and deep inelastic e^+p scattering are predominantly quark initiated, the similarity in the jet shapes indicates that the pattern of QCD radiation within a quark jet is to a large extent independent of the hard scattering process in these reactions.

Acknowledgements

The strong support and encouragement of the DESY Directorate have been invaluable. The experiment was made possible by the inventiveness and the diligent efforts of the HERA machine group. The design, construction and installation of the ZEUS detector have been made possible by the ingenuity and dedicated efforts of many people from inside DESY and from the home institutes who are not listed as authors. Their contributions are acknowledged with great appreciation.

References

- [1] CDF Collab., F. Abe et al., Phys. Rev. D45 (1992) 1448.
- [2] J. Huth et al., Proc. of the 1990 DPF Summer Study on High Energy Physics, Snowmass, Colorado, edited by E.L. Berger (World Scientific, Singapore,1992) p. 134.
- [3] S.D. Ellis, Z. Kunszt and D.E. Soper, Phys. Rev. Lett. 69 (1992) 3615.
- [4] S.J. Brodsky and J. Gunion, Phys. Rev. Lett. 37 (1976) 402; K. Shizuya and S.-H.H. Tye, Phys. Rev. Lett. 41 (1978) 787; M.B. Einhorn and B.G. Weeks, Nucl. Phys. B146 (1978) 445.
- [5] OPAL Collab., G. Alexander et al., Phys. Lett. B265 (1991) 462; OPAL Collab., P.D. Acton et al., Z. Phys. C58 (1993) 387; OPAL Collab., R. Akers et al., Z. Phys. C68 (1995) 179; OPAL Collab., G. Alexander et al., Z. Phys. C69 (1996) 543; DELPHI Collab., P. Abreu et al., Z. Phys. C70 (1996) 179; ALEPH Collab., D. Buskulic et al., Phys. Lett. B384 (1996) 353.
- [6] CDF Collab., F. Abe et al., Phys. Rev. Lett. 70 (1993) 713.
- [7] DØ Collab., S. Abachi et al., Phys. Lett. B357 (1995) 500.
- [8] W.T. Giele, E.W.N. Glover and D.A. Kosower, Nucl. Phys. B403 (1993) 633.
- [9] OPAL Collab., R. Akers et al., Z. Phys. C63 (1994) 197.
- [10] ZEUS Collab., J. Breitweg et al, Eur. Phys. J. C2 (1998) 61.
- [11] G. Kramer and S.G. Salesch, Phys. Lett. B317 (1993) 218 and Phys. Lett. B333 (1994) 519; M. Klasen and G. Kramer, Phys. Rev. D56 (1997) 2702.

- [12] ZEUS Collab., M. Derrick et al., Phys. Lett. B306 (1993) 158, Z. Phys. C67 (1995) 81 and Phys. Lett. B363 (1995) 201.
- [13] H1 Collab., I. Abt et al., Z. Phys. C61 (1994) 59 and Phys. Lett. B346 (1995) 415.
- [14] ZEUS Collab., M. Derrick et al., Z. Phys. C72 (1996) 47.
- [15] ZEUS Collab., M. Derrick et al., Phys. Lett. B293 (1992) 465.
- [16] The ZEUS Detector, Status Report 1993, DESY 1993.
- [17] ZEUS Collab., J. Breitweg et al., Z. Phys. C74 (1997) 207.
- [18] ZEUS Collab., M. Derrick et al., Z. Phys. C72 (1996) 399.
- [19] H. Abramowicz, A. Caldwell and R. Sinkus, Nucl. Inst. Meth. A365 (1995) 508.
- [20] S. Bentvelsen, J. Engelen and P. Kooijman, Proceedings of the Workshop on Physics at HERA, ed. W. Buchmüller and G. Ingelman (DESY, Hamburg, 1992), Vol. 1, p. 23.
- [21] Method proposed by F. Jacquet and A. Blondel in Proc. of the Study for an *ep* Facility for Europe, U. Amaldi et al., DESY 79/48 (1979) 377.
- [22] G. Ingelman, Proceedings of the Workshop on Physics at HERA, ed. W. Buchmüller and G. Ingelman (DESY, Hamburg, 1992), Vol. 3, p. 1366.
- [23] K. Kwiatkowski, H. Spiesberger and H.-J. Möhring, Proceedings of the Workshop on Physics at HERA, ed. W. Buchmüller and G. Ingelman (DESY, Hamburg, 1992), Vol. 3, p. 1294.
- [24] G. Schuler and H. Spiesberger, Proceedings of the Workshop on Physics at HERA, ed. W. Buchmüller and G. Ingelman (DESY, Hamburg, 1992), Vol. 3, p. 1419.
- [25] H.L. Lai et al., Phys. Rev. D55 (1997) 1280.
- [26] Y. Azimov, Y. Dokshitzer, V. Khoze and S. Troyan, Phys. Lett. B165 (1985) 147; G. Gustafson, Phys. Lett. B175 (1986) 453; G. Gustafson and U. Petersson, Nucl. Phys. B306 (1988) 746; B. Andersson, G. Gustafson and L. Lönnblad, Z. Phys. C43 (1989) 625.
- [27] L. Lönnblad, Comp. Phys. Comm. 71 (1992) 15 and Z. Phys. C65 (1995) 285.
- [28] H.-U. Bengtsson and T. Sjöstrand, Comp. Phys. Comm. 46 (1987) 43; T. Sjöstrand, Comp. Phys. Comm. 82 (1994) 74.
- [29] A.D. Martin, W.J. Stirling and R.G. Roberts, Phys. Rev. D50 (1994) 6734.
- [30] B. Andersson et al., Phys. Rep. 97 (1983) 31.
- [31] ZEUS Collab., M. Derrick et al., Phys. Lett. B342 (1995) 417.
- [32] M. Martínez, Ph.D. Thesis, Universidad Autónoma de Madrid (1998).
- [33] J.F. Owens, Phys. Rev. D21 (1980) 54.

- [34] W.J. Stirling and Z. Kunszt, Proceedings of the HERA Workshop (1987) 331; M. Drees and F. Halzen, Phys. Rev. Lett. 61 (1988) 275; M. Drees and R.M. Godbole, Phys. Rev. D39 (1989) 169.
- [35] ZEUS Collab., M. Derrick et al., Phys. Lett. B322 (1994) 287 and Phys. Lett. B348 (1995) 665.
- [36] E.W.N. Glover and D.A. Kosower, Phys. Lett. B367 (1996) 369.

ZEUS 1995

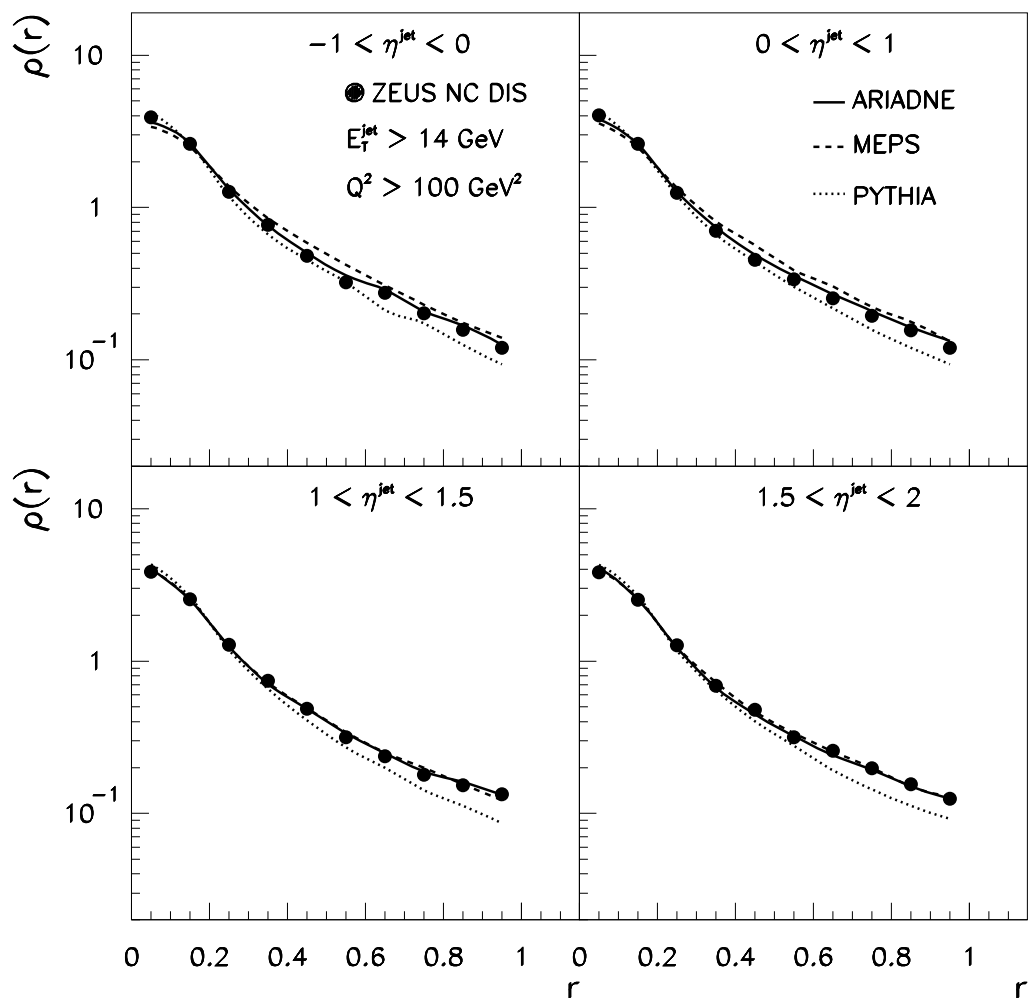


Figure 1: Measured differential jet shapes corrected to the hadron level, $\rho(r)$, in neutral-current DIS with $Q^2 > 100 \text{ GeV}^2$ for jets with E_T^{jet} above 14 GeV in different η^{jet} regions (black dots). The error bars include the statistical and systematic uncertainties added in quadrature (typically smaller than the dots). The predictions of PYTHIA (dotted lines), ARIADNE (solid lines), and MEPS (dashed lines) are shown for comparison. The predictions have been obtained by an integration over the same bins as for the data and are presented as smooth curves joining the calculated points.

ZEUS 1995

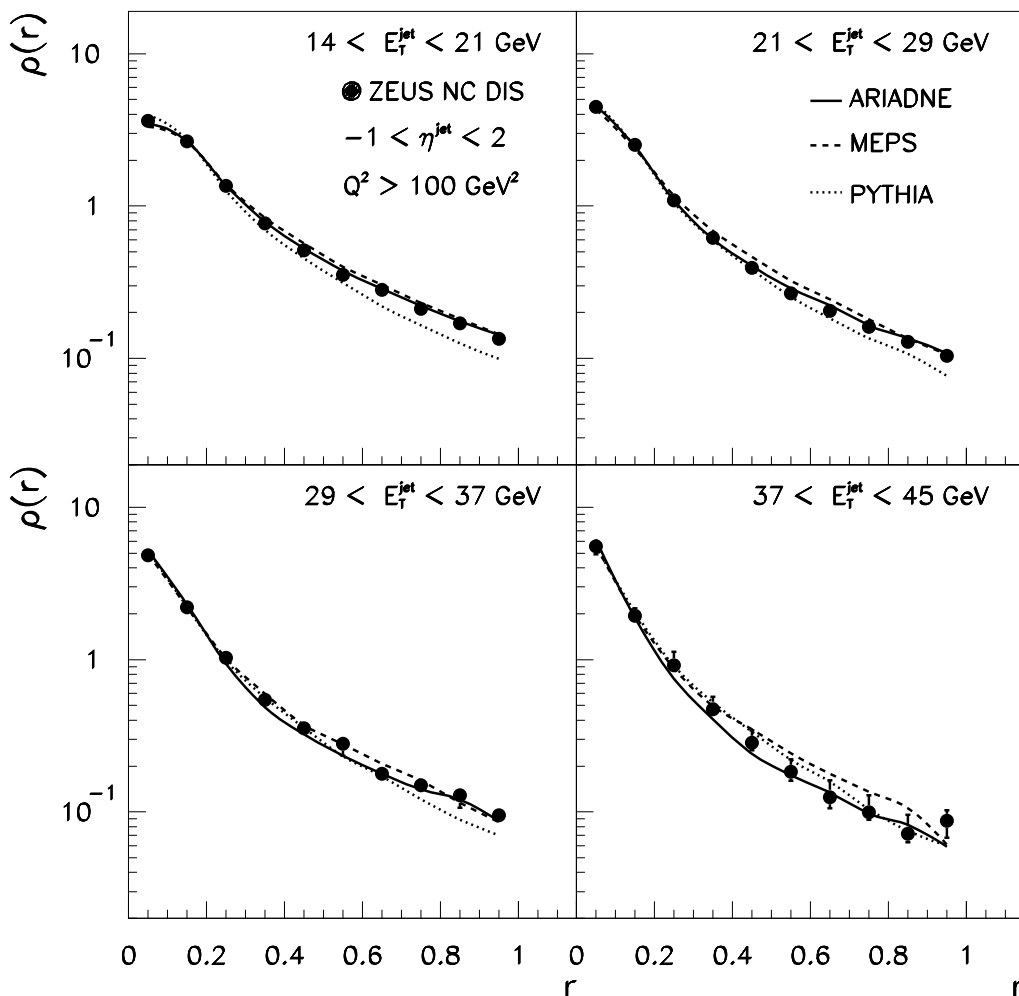


Figure 2: Measured differential jet shapes corrected to the hadron level, $\rho(r)$, in neutral-current DIS with $Q^2 > 100 \text{ GeV}^2$ for jets in the η^{jet} range between -1 and 2 in different E_T^{jet} regions (black dots). The error bars include the statistical and systematic errors added in quadrature. The predictions of PYTHIA (dotted lines), ARIADNE (solid lines), and MEPS (dashed lines) are shown for comparison. The predictions have been obtained by an integration over the same bins as for the data and are presented as smooth curves joining the calculated points.

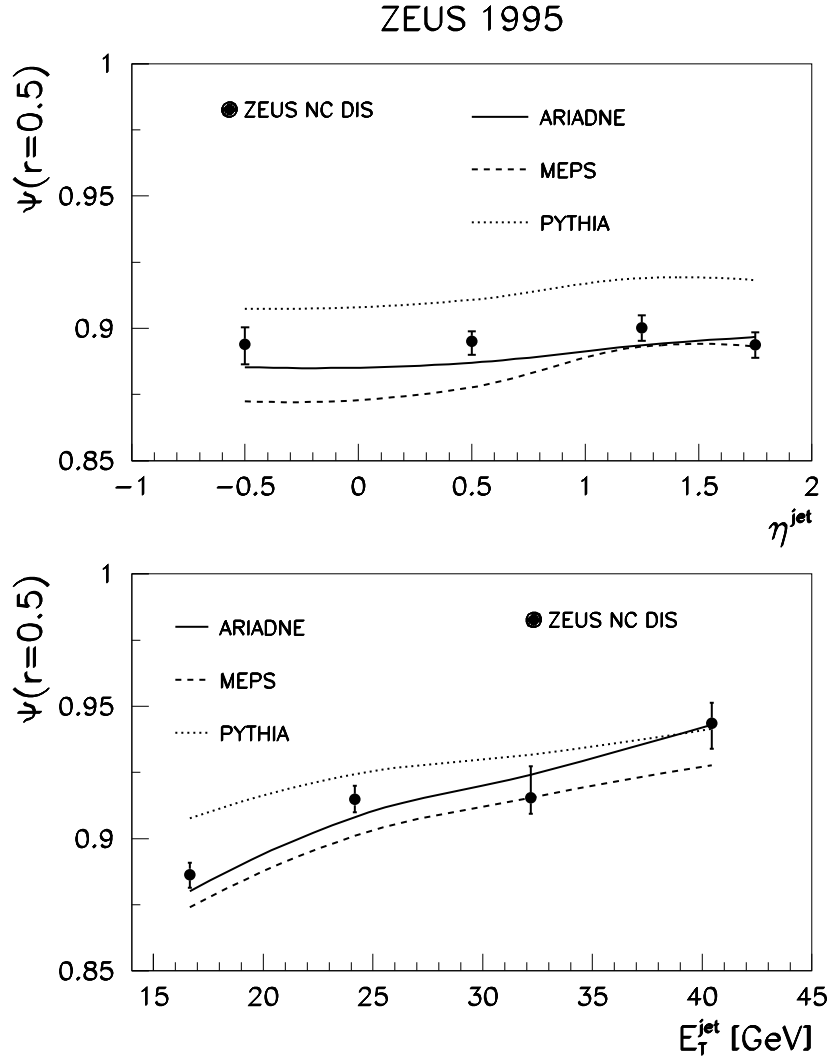


Figure 3: The measured integrated jet shape corrected to the hadron level at a fixed value of $r = 0.5$, $\psi(r = 0.5)$, as a function of η^{jet} (upper plot) and E_T^{jet} (lower plot), in neutral-current DIS with $Q^2 > 100 \text{ GeV}^2$ for jets with $E_T^{jet} > 14 \text{ GeV}$ in the η^{jet} range between -1 and 2 (black dots). The error bars include the statistical and systematic errors added in quadrature. The predictions of PYTHIA (dotted lines), ARIADNE (solid lines), and MEPS (dashed lines) are shown for comparison. The predictions have been obtained by an integration over the same bins as for the data and are presented as smooth curves joining the calculated points.

ZEUS 1995+1996

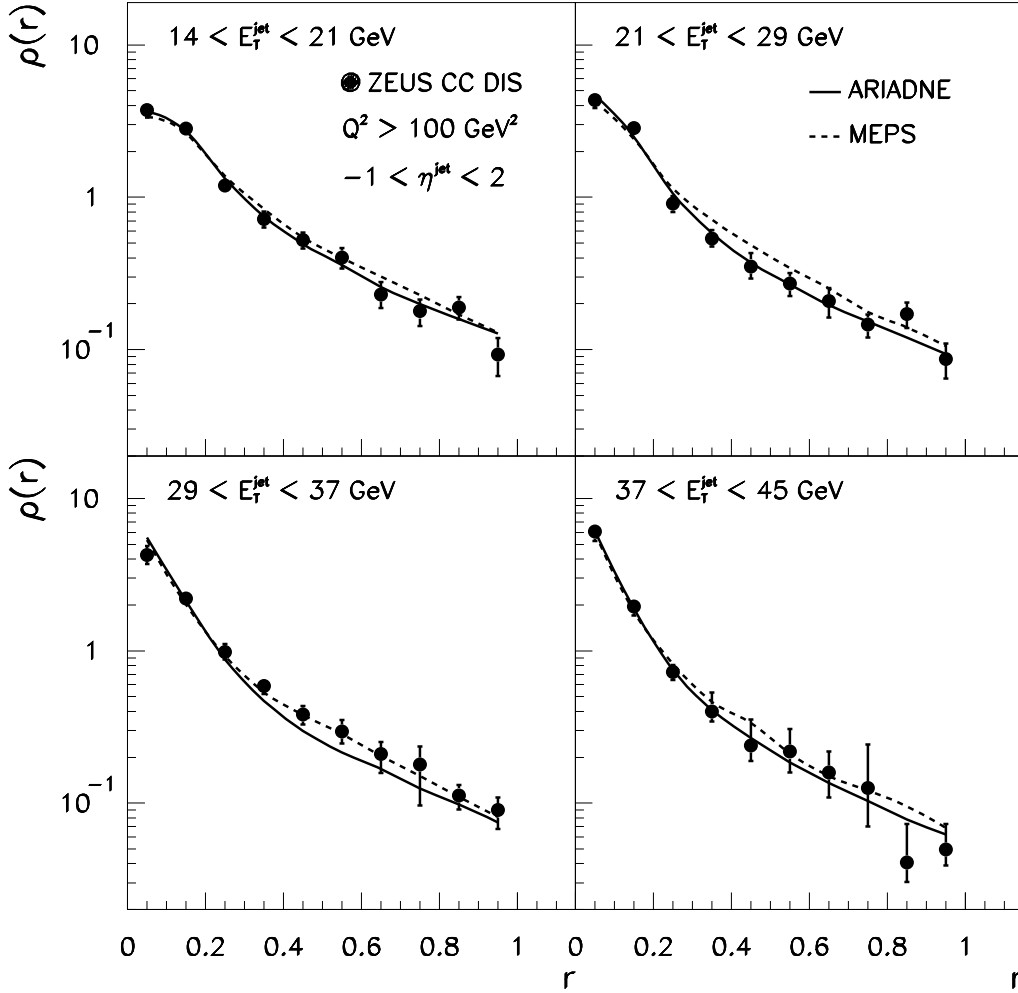


Figure 4: Measured differential jet shapes corrected to the hadron level, $\rho(r)$, in charged-current DIS with $Q^2 > 100$ GeV² for jets with $-1 < \eta^{jet} < 2$ in different E_T^{jet} regions (black dots). The predictions of ARIADNE (solid lines) and MEPS (dashed lines) are shown for comparison. The predictions have been obtained by an integration over the same bins as for the data and are presented as smooth curves joining the calculated points.

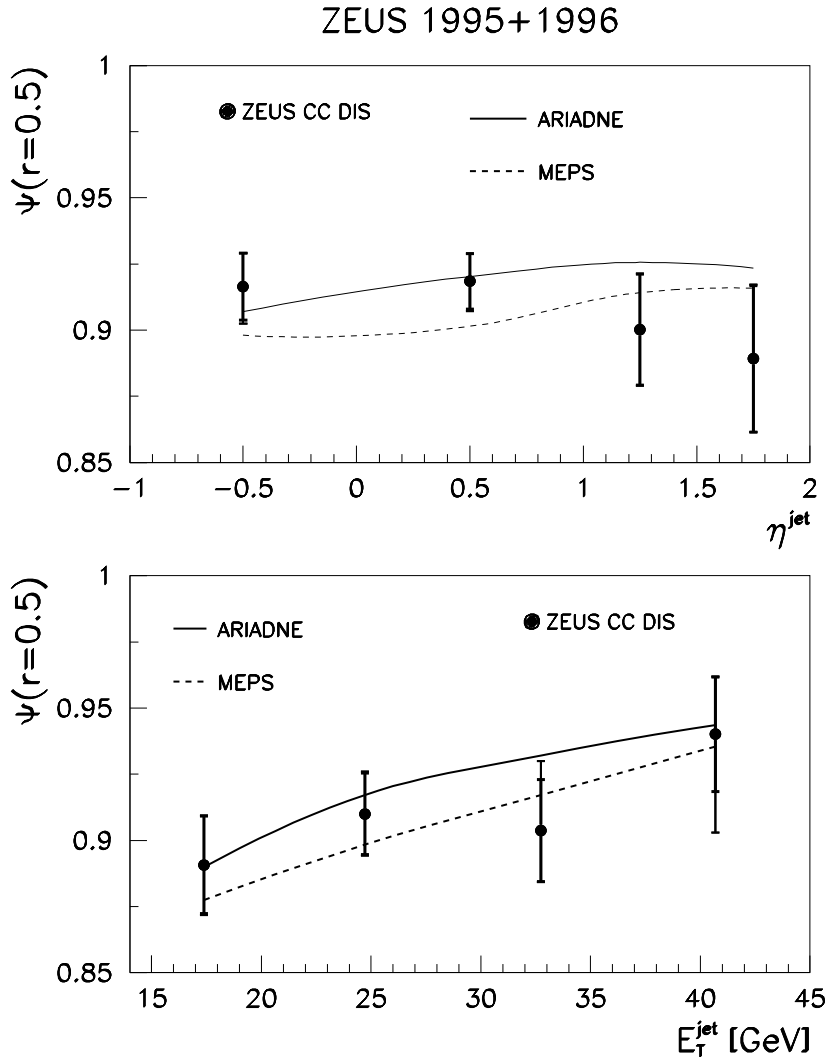


Figure 5: The measured integrated jet shape corrected to the hadron level at a fixed value of $r = 0.5$, $\psi(r = 0.5)$, as a function of η^{jet} (upper plot) and E_T^{jet} (lower plot), in charged-current DIS with $Q^2 > 100 \text{ GeV}^2$ for jets with $E_T^{jet} > 14 \text{ GeV}$ in the η^{jet} range between -1 and 2 (black dots). The inner error bars represent the statistical errors of the data, and the outer error bars show the statistical and systematic uncertainties added in quadrature. The predictions of ARIADNE (solid lines) and MEPS (dashed lines) are shown for comparison. The predictions have been obtained by an integration over the same bins as for the data and are presented as smooth curves joining the calculated points.

ZEUS 1995+1996

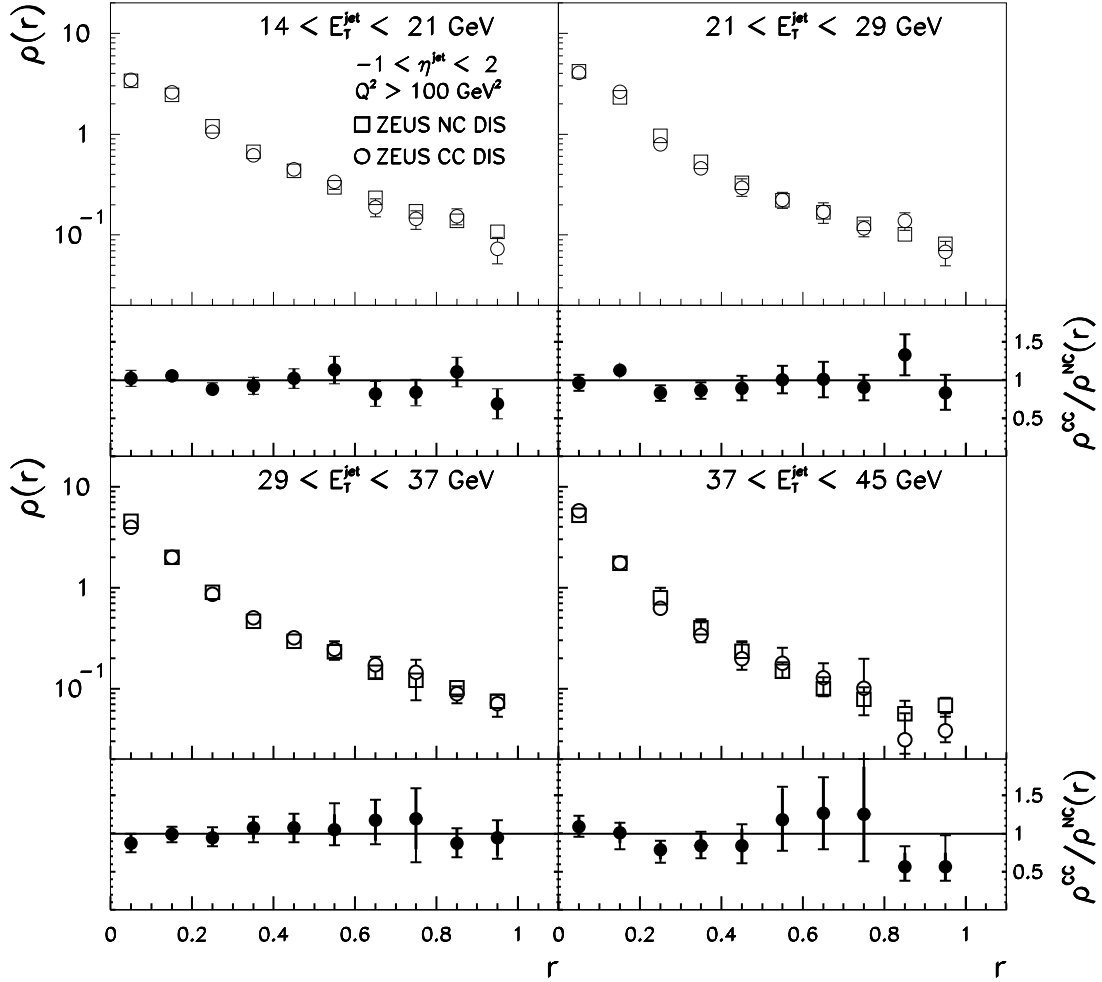


Figure 6: Measured differential jet shapes corrected to the hadron level, $\rho(r)$, in charged-current DIS with $Q^2 > 100$ GeV² for jets with $-1 < \eta^{jet} < 2$ in different E_T^{jet} regions (open circles). The measured jet shapes corrected to the hadron level for jets in neutral-current DIS with $Q^2 > 100$ GeV² with $-1 < \eta^{jet} < 2$ are shown for comparison (open squares). Measurements of the ratio $\rho^{CC}(r)/\rho^{NC}(r)$ are shown underneath each plot. The inner error bars represent the statistical errors of the data, and the outer errors bars show the statistical and systematic uncertainties added in quadrature.

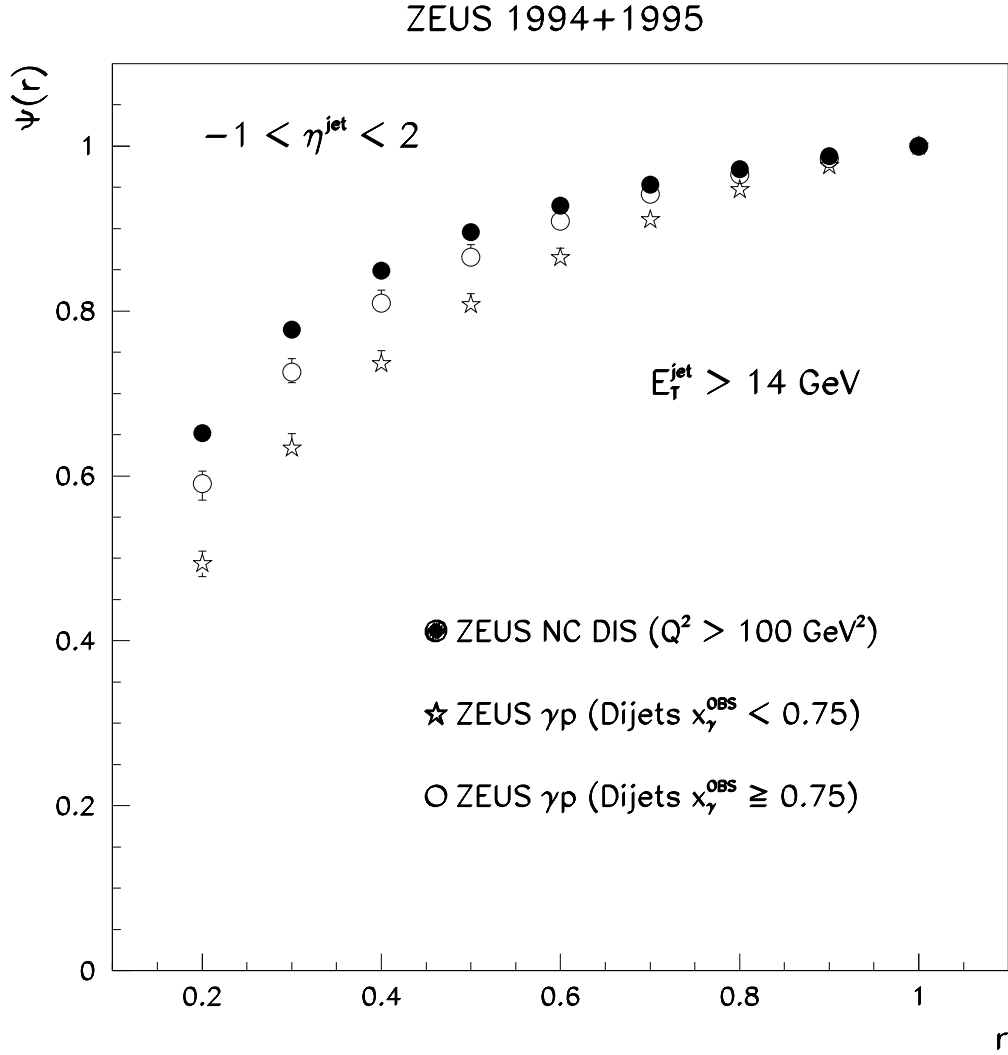


Figure 7: Measured integrated jet shape corrected to the hadron level, $\psi(r)$, in neutral-current DIS with $Q^2 > 100 \text{ GeV}^2$ for jets with E_T^{jet} above 14 GeV and $-1 < \eta^{jet} < 2$ (black dots). The measured jet shape corrected to the hadron level for jets in dijet photoproduction with E_T^{jet} above 14 GeV and $-1 < \eta^{jet} < 2$ is shown for comparison: for dijet production with $x_\gamma^{OBS} < 0.75$ (stars) and for dijet production with $x_\gamma^{OBS} \geq 0.75$ (open circles).

ZEUS 1995+1996

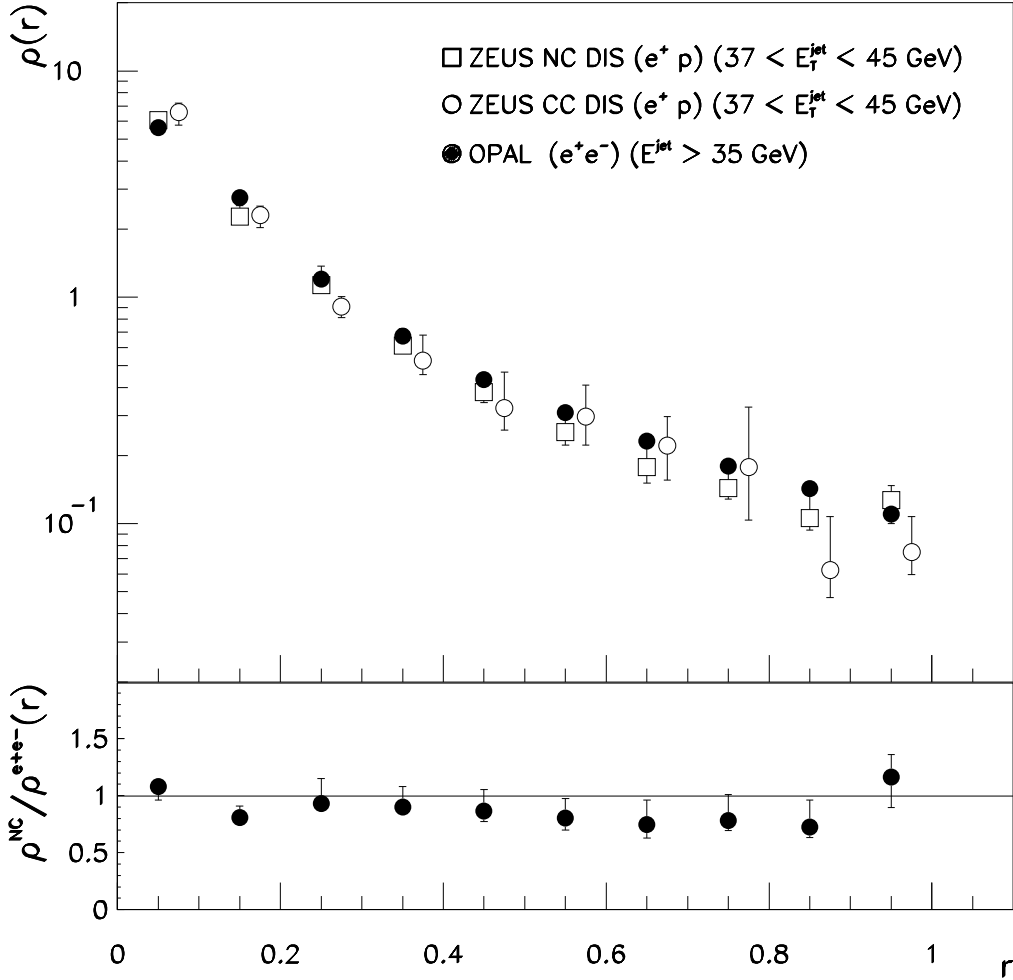


Figure 8: Measured differential jet shapes corrected to the hadron level, $\rho(r)$, in neutral- (charged-) current DIS with $Q^2 > 100$ GeV² and a median of 2000 GeV² (2200 GeV²) for jets with η^{jet} in the range between -1 and 2 and $37 < E_T^{jet} < 45$ GeV are shown as squares (open circles). The measurements in CC DIS have been obtained for the same values of r as those in NC DIS, and for an easier comparison the measurements are plotted at $r + 0.025$. The measurements of the jet shape in e^+e^- interactions by OPAL (black dots) is shown for comparison. The ratio of differential jet shapes in NC DIS and e^+e^- interactions, $\rho^{NC}(r)/\rho^{e^+e^-}(r)$, is shown in the lower part of the figure.

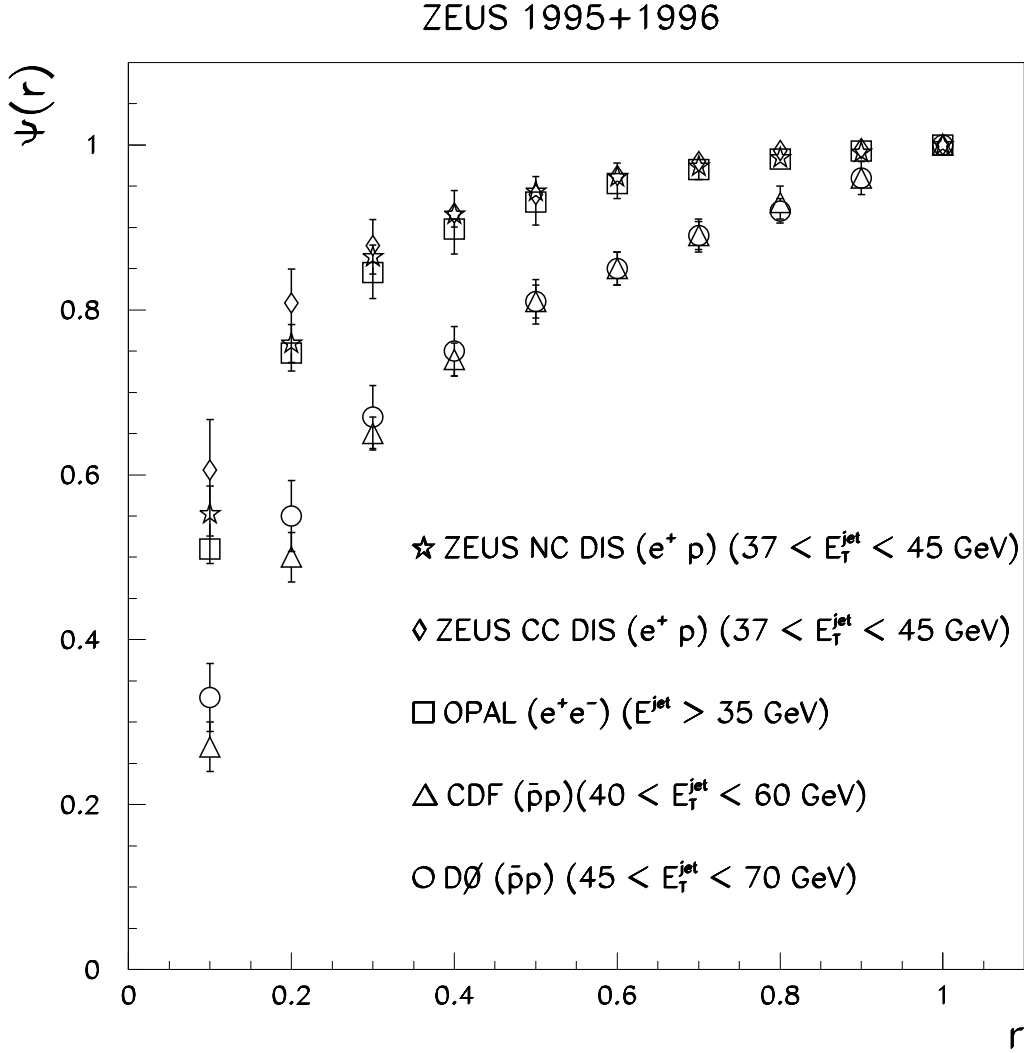


Figure 9: Measured integrated jet shapes corrected to the hadron level, $\psi(r)$, in neutral-(charged-) current DIS with $Q^2 > 100$ GeV² for jets with η^{jet} in the range between -1 and 2 and $37 < E_T^{jet} < 45$ GeV are shown as stars (diamonds). The measurements of jet shapes in $\bar{p}p$ collisions by CDF (triangles) and DØ (circles) and in e^+e^- interactions by OPAL (squares) are shown for comparison.